

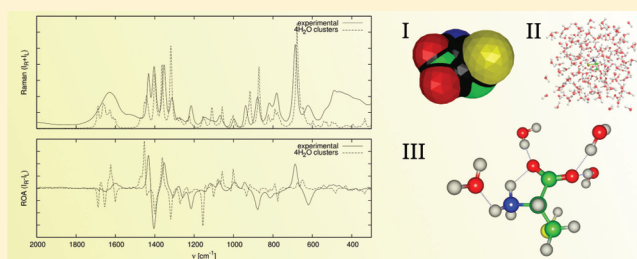
Vibrational Optical Activity of Cysteine in Aqueous Solution: A Comparison of Theoretical and Experimental Spectra

Maciej Kamiński, Andrzej Kudelski, and Magdalena Pecul*

Faculty of Chemistry, University of Warsaw, Pasteura 1, 02-093 Warszawa, Poland

S Supporting Information

ABSTRACT: Raman, Raman optical activity (ROA), infrared (IR), and vibrational circular dichroism (VCD) spectra of cysteine in aqueous solution have been measured and calculated by means of density functional theory. The influence of aqueous environment on the spectra of cysteine has been simulated by means of implicit (polarizable continuum model) and explicit (molecular dynamics, solute–solvent clusters) methods. The results indicate that, while PCM reproduces some of the features of the spectra, the best description is rendered by the microsolvation model (solute–solvent clusters). The shape of the bands is in some cases more correctly reproduced by MD, but their intensities and positions are not, since these simulations are hampered by the standard force field being parametrized for conformations of peptides rather than isolated amino acids. The calculated ROA spectra have been used to extract conformational ratios from the experimental spectra, and again, the best results (as verified by simulations of other spectra) have been obtained when using the microsolvation model. This procedure renders three zwitterion conformers dominating the spectra of hydrated cysteine, of conformational ratios of 35, 33, and 24%, respectively.



I. INTRODUCTION

Vibrational chiroptical spectroscopies: Raman optical activity (ROA) and vibrational circular dichroism (VCD) are very sensitive probes of molecular structure, capable of providing information not only on the absolute configuration of a molecule^{1–14} but also about its conformational space, dynamics, and interactions with environment.^{15–20} They have been used to provide information on a wide range of chemical systems, from small organic molecules^{11,12,20} to proteins,^{19,21–23} nucleic acids,^{22,24,25} and nucleic acid–protein complexes.^{22,24,26}

The main advantage of vibrational chiroptical spectroscopies over the more established chiroptical methods relying on optical rotation (OR) or electronic circular dichroism (CD) is that they provide more information: in principle, each vibrational peak can be used for structural analysis, while in the case of electronic spectra we usually have at our disposal only one number (OR at a single wavelength) or at best a few (if rotatory strengths for several electronic transitions are available from the circular dichroism spectrum). As a consequence, the likelihood of erroneous assignment of absolute configuration from VCD or ROA spectra is smaller than in the case of circular dichroism or optical rotatory dispersion spectra. However, there are no empirical rules relating the sign and magnitude of observed ROA or VCD intensities to the molecular structure, and the use of ROA and VCD for assignment of an unknown absolute configuration of an optically active molecule or for deriving information about conformations of a flexible optically active molecule relies strongly on quantum chemical calculations.

The very sensitivity of VCD and ROA spectra to conformational changes and influence of the environment, which makes them good indicators of molecular structures,^{17,27–29} causes quantum chemical calculations of them to be a challenging task, especially in the case of flexible molecules with polar group in aqueous environment. In addition to the usual problem of adequate modeling of the electronic structure (such as electron correlation or basis set size), one needs also to be concerned about probing the whole conformational space and accounting for all low-energy conformers, and, what is even more problematic, about taking into account solvent effects. There are two methods used nowadays for the latter purpose: (a) implicit solvent models,^{28,30,31} in which the solvent is described as a continuous medium, dielectric^{32–34} or conductor-like,^{35–37} or as a discrete distribution of charges^{38,39} and (b) explicit solvent models, in which quantum chemical calculations are carried out for a cluster containing the molecule of interest surrounded by solvent molecules rather than for an isolated chiral molecule.^{40–43} The structures of such a cluster can be generated either by manually adding solute molecules and carrying out geometry optimization (a cost-effective approach but in danger of creating an unphysical bias because of the omission of some structures) or by molecular dynamics simulations. It has been recently shown⁴⁰ that explicit solvent models are superior to implicit solvent models in rendering the ROA spectra of

Received: January 20, 2012

Revised: March 27, 2012

Published: March 27, 2012

hydrated hydrogen-bond-forming molecules: lactamide and aminopropanol. Similar conclusions have been drawn by other authors.^{42,43} It has also been demonstrated in ref 40 that the best results are obtained when Carr–Parinello molecular dynamics is used, provided the simulation time is long enough to allow the system to probe the full conformational space, a task which is, however, of prohibitive computational cost for flexible molecules in aqueous environment. Thus, in the present work, we decided not to perform quantum molecular dynamics calculations and limit our calculations to classical molecular dynamics. We focus here instead on simultaneous examination of the performance of implicit (polarizable continuum) and explicit (manually constructed solute–solvent clusters and clusters from MD calculations) solvent model in rendering of both ROA and VCD spectra. We also demonstrate how the ROA spectra can be used to determine conformational ratios.

The system under study is cysteine, selected on the basis of its small size and interesting vibrational spectrum resulting from the presence of the thiol group. Vibrational chiroptical spectra of cysteine have been a subject of several experimental and theoretical studies.^{44–48} ROA spectra of cysteine have been recently shown in ref 45, where the spectra of cysteine in aqueous solution and spectra of the silver surface covered by the cysteine monolayer have been demonstrated. In the present study, we have carried out measurements of the ROA and VCD spectra of both enantiomers of cysteine in aqueous solutions (in D₂O in the case of VCD spectra) and quantum chemical calculations of them, simulating the solvent by means of implicit and explicit methods.

The paper is organized as follows. After the description of the computational methods and experimental setup, we discuss the cysteine conformers derived from geometry optimization and molecular dynamics, and then we proceed to the discussion of experimental and theoretical Raman and ROA spectra. We examine the performance of polarizable continuum model, micro-solvation model, and molecular dynamics in simulating the influence of aqueous environment on the spectra, and propose a technique of deriving conformational ratios from the experimental spectra. The discussion of performance of solvent models is then repeated for IR and VCD spectra. Finally, a summary is presented and some conclusions are drawn.

II. EXPERIMENTAL AND COMPUTATIONAL DETAILS

A. Experiment. To measure ROA (and classical Raman) spectra of cysteine, 1 M solutions of L- and D-cysteine in water have been prepared and poured into 4 mm optical path length quartz cuvettes and the spectra have been measured using a ChiralRAMAN spectrometer from BioTools with a resolution of ca. 4 cm^{−1}, partially based on the design described by Werner Hug.^{49,50} (The schematic optical design of the BioTools Chiral RAMAN instrument can be found in refs 21 and 51.) The acquisition time is approximately 12 h for one sample with incident laser radiation of 532 nm wavelength and 2 W beam power.

Infrared absorbance and VCD measurements have been performed on a Nicolet 8700 FTIR spectrometer equipped with a VCD optical bench. The spectrometer and the VCD optical bench have been purged with dry air. The main elements of the VCD optical bench are the following: wire grid polarizer, ≈50 kHz photoelastic modulator, ≈50 kHz synchronous sampling demodulator (SSD), and a mercury–cadmium–telluride (MCT) liquid-nitrogen-cooled detector. A more detailed description of the FT-VCD setup may be found

in refs 52 and 53. VCD spectra have been collected at room temperature with a resolution of 4 cm^{−1} in the spectral range 800–1900 cm^{−1} (a low pass filter cutting away the signals above 1975 cm^{−1} has been used to increase the sensitivity of the measurement). A total of 10000 scans at 4 cm^{−1} resolution using Happ–Ganzel hapodization have been averaged to obtain each spectrum. For all experiments, a transmission cell for liquid samples equipped with BaF₂ windows and ca. 12 μm thick spacers has been used.

For the IR/VCD measurements, cysteine with labile protons exchanged for deuterons has been prepared by two cycles involving dissolution of cysteine in heavy water (99.9% D₂O) and the subsequent evaporation of the solvent in rotary evaporator under the pressure of ca. 3 kPa. Finally, a saturated cysteine solution has been prepared and the IR/VCD spectra have been measured. Due to the strong absorption, the signal at 1621 cm^{−1} has been obtained in a separate VCD measurement for a solution diluted three times with D₂O.

To check whether cysteine does not form dimers in neutral solution or significantly oxidizes during the experiment, Raman and ROA spectra of 0.25 M L-cysteine solution and Raman and ROA spectra of saturated cysteine solution have been measured using techniques analogous to these described earlier and compared with the spectra of 1 M cysteine solution.

B. Calculations. *a. Calculations with the Implicit Solvent Model.* First, we have performed a search for the energetically lowest conformers of cysteine in water modeled as a dielectric continuum. We have assumed (on the basis of the dissociation constants of cysteine⁵⁴ and pH of neutral cysteine solution equal approximately to 5.3) that cysteine molecules in neutral aqueous environment exist only in the zwitterionic form, i.e., that the optical spectra come only from molecules in their zwitterionic forms.

Trial structures of zwitterionic cysteine have been generated using all combinations of the following dihedral angles (see Figure 1): 0 and 60° for the –NH₃⁺ group (δ angle – defined

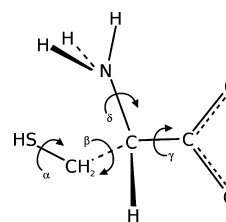


Figure 1. Nomenclature of dihedral angles in cysteine. The angles are defined by the positions of the atoms as follows: α , H–S–C_β–C_α; β , S–C_β–C_α–C=O; γ , C_β–C_α–C=O–O; δ , C_β–C_α–N–H.

by the positions of the C_β, C_α, N, and H atoms); 0, 60, 120, 180, 240, and 300° for the –SH group (α angle – H, S, C_β, C_α); 0, 60, and 120° for the anionic carboxyl group (γ angle – C_β, C_α, C=O, O); and 0, 60, 120, 180, 240, and 300° for the angle between C_α and C_β (β angle – S, C_β, C_α, C=O) which resulted in 216 different conformers. A similar procedure was employed in refs 55 and 56. The geometry of the conformers has been initially optimized using DFT (with the B3LYP functional and 3-21+G* basis set), and the solvent environment has been simulated by means of the IEF-PCM model (with alpha scaling factor 1.2 and sphere radii default in Gaussian 03⁵⁷). The obtained set of different structures (structures were assumed different when the dihedral angle varied more than by 10°) has been subjected again to geometry optimization, this time with

the aug-cc-pVDZ basis set. 216 initial geometries converged finally to eight structures, although only seven of them represent energy minima. ROA, Raman, VCD, and IR intensities have been calculated only for five structures with abundancies greater than 1% (as obtained from Boltzmann distribution) using the same computational model as for the final geometry optimization. The resulting spectra have been simulated using Lorentzian function fitting with 10 cm^{-1} halfwidth and Boltzmann averaging. For calculation of VCD and IR spectra, labile protons have been replaced with deuterons, since the experimental VCD spectra of cysteine have been measured in heavy water solution. The conformational ratios have been calculated from the Boltzmann distribution obtained from free enthalpies.

All calculations have been carried out using Gaussian 03⁵⁷ and Gaussian 09⁵⁸ computational programs.

b. Microsolvation Model. Another approach to model the water environment has been to add manually four water molecules to each of the five zwitterionic structures of cysteine obtained in the previous step. This has been done in five different ways for each of the conformers, resulting in 25 different cysteine–water clusters. Three water molecules have been placed in the vicinity of the carbonyl group, and one water molecule has been assumed to form hydrogen bonds with the amino group (see Figure S1 in the Supporting Information). The remaining aqueous environment has been simulated by means of IEF-PCM. The initial cluster structures have been optimized using DFT (with the B3LYP functional and aug-cc-pVDZ basis set), and the spectra of them have been calculated at the same level of theory. The spectra have been obtained by fitting Lorentzian functions to all of the signals and Boltzmann averaging over free enthalpies.

c. Molecular Dynamics Approach. To simulate an aqueous solution of cysteine in a more realistic manner, molecular dynamics with the AMBER02 force field has been used. Initially, the most stable conformer of cysteine molecule obtained from the implicit solvent approach has been placed in a 18.643 Å box containing 216 water molecules and the modified Beeman algorithm has been executed using the TINKER 5.1 molecular modeling package.⁵⁹ At first, 100 snapshots were extracted from the 500 ps, 5×10^5 steps dynamics run, but as the β angle was not changing during the run, the parameters were changed to 5 ns, 5×10^6 steps and then 100 structures with all water molecules closer than 2.3 Å were extracted from the snapshots. The obtained structures have been then subjected to normal mode geometry optimization (at the B3LYP/aug-cc-pVDZ level) using the QGRAD program⁶⁰ freezing all modes with a wavenumber below 300 cm^{-1} . ROA, Raman, IR, and VCD intensities have been calculated for all optimized structures, and then, the final spectra have been estimated using Lorentzian function fitting (again with 10 cm^{-1} halfwidth) and averaged. For calculation of VCD and

IR spectra, labile protons in cysteine and water have been replaced with deuterons.

III. RESULTS AND DISCUSSION

A. Cysteine Conformers. 1. Implicit Hydration Model.

The structures of the lowest zwitterion conformers of cysteine, as obtained by geometry optimization with the aqueous environment simulated by means of the IEF-PCM model, are shown in Figure 2, while their relative energies

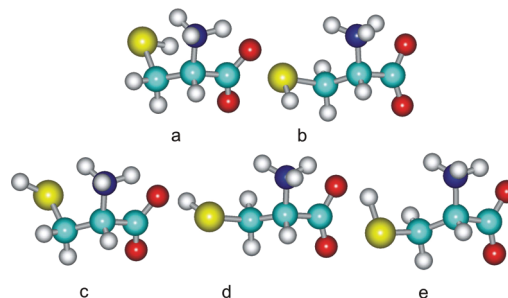


Figure 2. The structures of the most stable zwitterion conformers of cysteine as obtained by B3LYP/aug-cc-pVDZ geometry optimization with the IEF-PCM model.

ΔE , free energies ΔG , Boltzmann distribution factors (obtained from ΔG), and torsion angles (for the definitions of the angles, see Figure 1) are shown in Table 1. The values of ΔG and Boltzmann distribution factors are also given for the deuterated cysteine molecule, where labile protons have been replaced by deuterons. In both cases, the *a* conformer is the most abundant one, but the relative weight of the higher-energy conformers is increased upon deuteration.

It should be noted at this point that there are differences between the results obtained using IEF-PCM implementations in Gaussian 03 and Gaussian 09 (compare Table 1 and Table S1 in the Supporting Information): the Boltzmann weight of the most abundant conformer is 50.2% when using Gaussian 03 and 40.6% when using Gaussian 09, even though the cavity radii have been chosen the same. This comes mostly from different modeling of the cavity: in Gaussian 03, the code automatically adds spheres not centered on atoms which take into account the dimension of the solvent, while in Gaussian 09 no such spheres are added. Furthermore, the applied grid is somewhat different. These differences in IEF-PCM implementation in Gaussian 03 and Gaussian 09 affect mostly the calculated harmonic frequencies, and in turn the free energies. The consequences for the calculated vibrational spectra will be discussed later on.

The results obtained in this approach are similar to those from the work of Dobrowolski, Rode, and Sadlej.⁵⁶ The three

Table 1. Relative Energies (ΔE [kJ/mol]), Relative Free Enthalpies (ΔG for Normal Cysteine and ΔG_D for Deuterated Cysteine [kJ/mol]), Molar Fractions (*x*) Calculated from Boltzmann Distribution (Using ΔG and ΔG_D), and Cysteine Conformer Torsion Angles in Degrees

conformer	ΔE	ΔG	ΔG_D	<i>x</i> (ΔG)	<i>x</i> (ΔG_D)	α	β	γ	δ
<i>a</i>	0	0	0	0.50	0.43	66	289	134	96
<i>b</i>	2.98	1.81	1.40	0.23	0.25	298	188	110	14
<i>c</i>	5.16	3.15	2.72	0.13	0.14	248	291	135	100
<i>d</i>	7.56	5.06	3.77	0.06	0.09	145	181	113	11
<i>e</i>	7.71	4.63	4.02	0.07	0.08	84	172	125	109

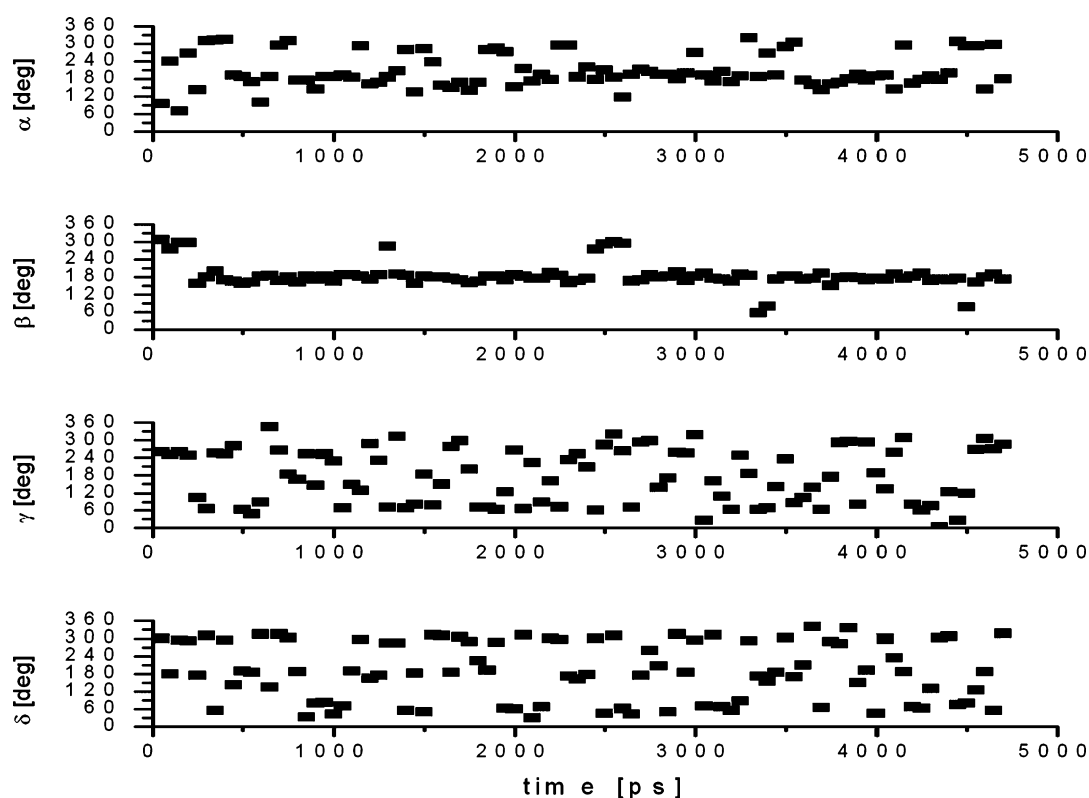


Figure 3. Angular distributions obtained from 5 ns MD run.

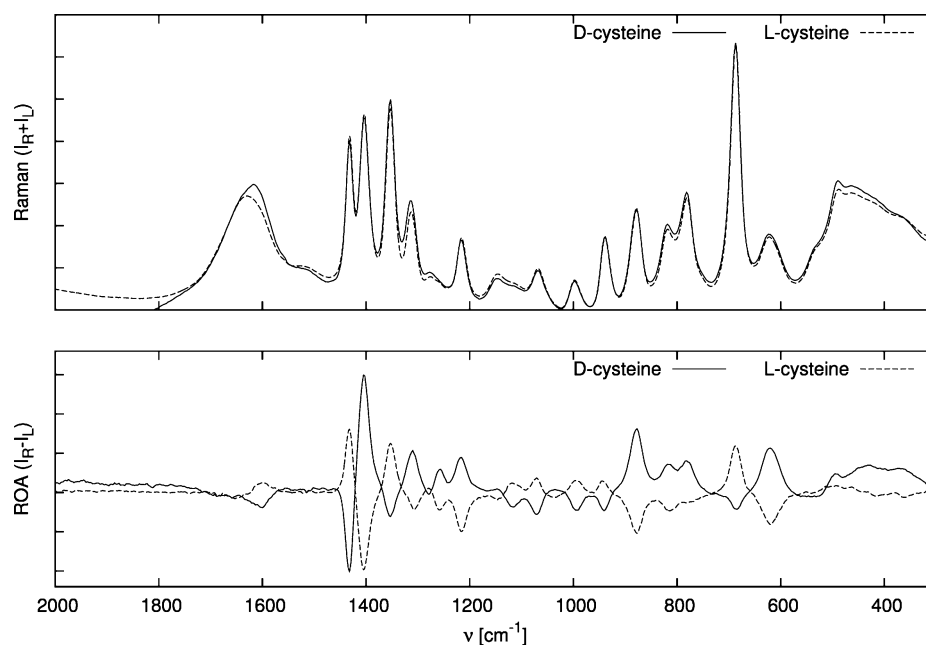


Figure 4. The experimental Raman (upper graph) and ROA (lower graph) spectra of 1 M aqueous solutions of L- and D-cysteine.

energetically lowest structures here correspond to three of four zwitterionic conformers of cysteine in ref S6—to the first, the second, and the fourth structure in the order of their raising energy. The third conformer of ref S6 has been found to converge to one of the structures with the abundance below 1% (0.02% to be precise).

2. Explicit Hydration Model. Two ways of generating cysteine–water clusters to model hydration have been employed: geometry optimization of cysteine (in zwitterion

conformation) with four water molecules and molecular dynamics.

a. Microsolvation Model. Geometry optimization of manually constructed cysteine–water clusters has not changed significantly the geometry parameters of the cysteine conformers, changing mostly the positions of the water molecules. However, the energy ordering of the explicitly hydrated clusters differs significantly from the IEF-PCM-only results. For instance, the most abundant (46%) structure has been obtained

Table 2. The Peak Assignment of the FTIR/VCD Spectrum of Cysteine in Heavy Water Solution on the Basis of Cys•4D₂O Clusters B3LYP/aug-cc-pVDZ Results

exp. ν (cm ⁻¹)	calc. ν (cm ⁻¹)	vibration type	ref 61: $\nu_{\text{exp.}}$ $\nu_{\text{calc.}}$ vib. type
1175	1180–1237 ^a	δ -D ₂ O, δ_s -ND ₃ ⁺ + δ -CH + τ -CH ₂	1170/95 ^b ; 1165/84; δ_{sa} -ND ₃ ⁺
1209		δ -D ₂ O of bulk liquid heavy water	
1298	1303	δ -CH (C _{α} -C _O plane) ^c + ω -CH ₂	1285; 1274; ω -CH ₂
1342	1355	δ -CH (C-N)	1358; 1356; δ -CH
1399	1395	ν_s -CO ₂ ⁻ + δ -CH (C-N) + δ -CH ₂	1398; 1400; -
1430	1431	δ -CH ₂	1426; 1437; δ -CH ₂
1621	1643	ν_a -CO ₂ ⁻	1576; 1588; ν_a -CO ₂ ⁻

^aA few signals inside the specified range. ^bTwo separate signals, e.g., 1170 and 1195 cm⁻¹. ^cCH bending vibrations along a plane containing the C _{α} -C_O bond.

from the conformer *d*, which is one of the least abundant among structures obtained in the implicit hydration approach. The relative energies ΔE of the clusters, their free energies ΔG , Boltzmann distribution factors (obtained from ΔG), and torsion angles along with the changes of the angles in relation to the original structures are shown in Table S2 in the Supporting Information. The Boltzmann distribution factors will be discussed in more detail later.

b. Molecular Dynamics Simulations. The angular distribution obtained in the course of the MD run is shown in Figure 3. Most of the structures generated in the MD simulation can be assigned to two groups: the structures in the first and the biggest group have $\beta \approx 180^\circ$ and $\alpha \approx 180^\circ$, and the second set has $\beta \approx 180^\circ$ and $\alpha \approx 300^\circ$. The γ angle of the structures from these groups is spread more or less uniformly. A few structures that cannot be assigned to either of these group almost exclusively have $\gamma \approx 60^\circ$. The geometry of the first group of structures is somewhat similar to the *d* conformer and the second group of structures is similar to the *b* conformer from the implicit solvation approach, but otherwise, there are no large similarities between the geometries from the two approaches.

B. Raman and ROA Spectra. **1. Experimental Spectra.** The experimental Raman and ROA spectra obtained for 1 M aqueous solutions of L- and D-cysteine are shown in Figure 4. The Raman spectra of both enantiomers practically superimpose each other, while the ROA spectra are mirror images of each other. The mirror symmetry indicates that there should be few artifacts in the ROA spectra. Since the applied concentration of cysteine was high (in order to obtain a ROA spectrum of good quality), we have also carried out the measurements for 0.25 M solution of L-cysteine, to check whether there are no changes of the spectrum with concentration, which would suggest a formation of cysteine dimers. The obtained Raman and ROA spectra (shown in Figure S2 in the Supporting Information) are essentially identical with those for 1 M solution of L-cysteine, apart from higher spectral noise and higher intensity of the water signal. Therefore, the contribution from cysteine dimers at these concentrations is negligible. The other additional experiment we have attempted to carry out has been a measurement of cystine spectrum, carried out in order to assess the role of possible contributions from a product of cysteine oxidation. However, the solubility of cystine under the experimental conditions is so low that no ROA spectrum could be

Table 3. The Peak Assignment of the Raman/ROA Spectrum of Cysteine in Aqueous Solution on the Basis of Cys•4H₂O Clusters B3LYP/aug-cc-pVDZ Results

exp. ν (cm ⁻¹)	calc. ν (cm ⁻¹)	vibration type	ref 61: $\nu_{\text{exp.}}$ $\nu_{\text{calc.}}$ vib. type
≈ 534	530	backbone	535; 535; -
622	615	backbone (i.a. δ -CO ₂ ⁻)	638; 635; δ -CO ₂ ⁻
687	670	ν -CS	691; 687; ν -CS
781	768	backbone	
	790	backbone	773; 795; -
818	814	δ/ω -CO ₂ ⁻	826; 827; ω -CO ₂ ⁻
878	874	backbone	868; 883; -
939	916	δ -SH + ν_a -C _O C _{α} N + τ -CH ₂	931; 922; -
997	1008	ρ -NH ₃ ⁺ + ν -C _{β} C _{α} + ρ -CH ₂ + δ -SH	1004; 1008; -
1069	1063	i.a. ν_a -C _{β} C _{α} N	
1117	1114		1106; 1103; -
1146	1147	ρ -NH ₃ ⁺ + δ -CH (vibrations in two directions)	1140; 1144; ρ -NH ₃ ⁺
1216	1213	δ -CH (C _{α} -C _O plane) ^a + τ -CH ₂	-; 1258; τ -CH ₂
1276	1289	ω -CH ₂	1269; 1278; ω -CH ₂
1313	1308	δ -CH (C _{α} -C _O) + ω -CH ₂	1303; 1322; -
1353	1360	δ -CH (C-N)	1344; 1356; δ -CH
1404	1396	ν_s -CO ₂ ⁻ + δ -CH (C-N) + δ -CH ₂	1397; 1410; -
1432	1430	δ -CH ₂	1424; 1439; δ -CH ₂
1524	1470	δ_s -NH ₃ ⁺	1523; 1524; δ_s -NH ₃ ⁺
1630	1613–1700 ^b	δ -H ₂ O, δ_a -NH ₃ ⁺ , ν_a -CO ₂ ⁻	1575; 1588; ν_a -CO ₂ ⁻ 1641; 1642/45; δ_a -NH ₃ ⁺

^aCH bending vibrations along a plane containing the C _{α} -C_O bond.

^bA few signals inside the specified range.

recorded, so the presence of cystine (if any) in cysteine solution should not have a strong influence on the spectrum.

The signals visible in the IR/VCD and Raman/ROA spectra are ascribed to normal vibrations in Tables 2 and 3 on the basis of the calculations with cysteine–water clusters (see below), and any further discussion of the signals will be based on this ascription. Vibrational modes have been described as follows: ν – stretching mode, a/s indices – antisymmetric/symmetric mode, δ – bending (usually scissoring) mode, ω – wagging mode, ρ – rocking mode, and τ – twisting mode.

The peak assignments have also been compared in Tables 2 and 3 to the reference work⁶¹ in which vibration modes of polycrystalline cysteine powder have been studied using isotopic substitution aided by computational methods. Vibration assignments presented here are practically identical to these in the reference, though in some places they are more detailed and have filled a few gaps.

2. PCM Model. The Raman and ROA spectra calculated with the aqueous environment simulated by means of the implicit polarizable continuum model are compared with experimental spectra in Figure 5.

In the spectral region up to 900 cm⁻¹, both theoretical Raman and ROA spectra share a lot of similarity with the corresponding

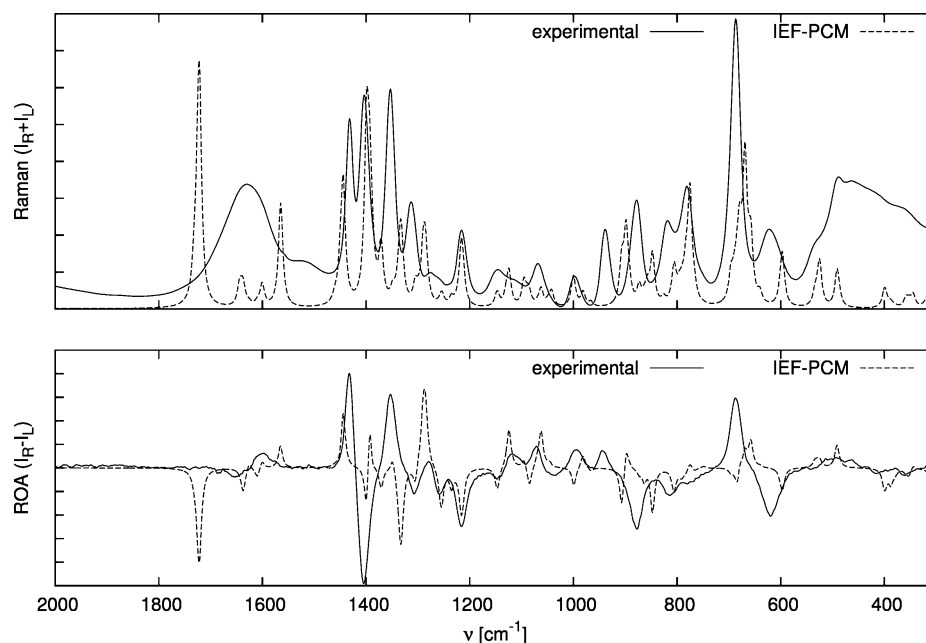


Figure 5. Comparison of the Raman (upper graph) and ROA (lower graph) spectra of L-cysteine obtained simulating aqueous environment by means of the PCM model implemented in Gaussian 03 (dashed line) with experiment (solid line).

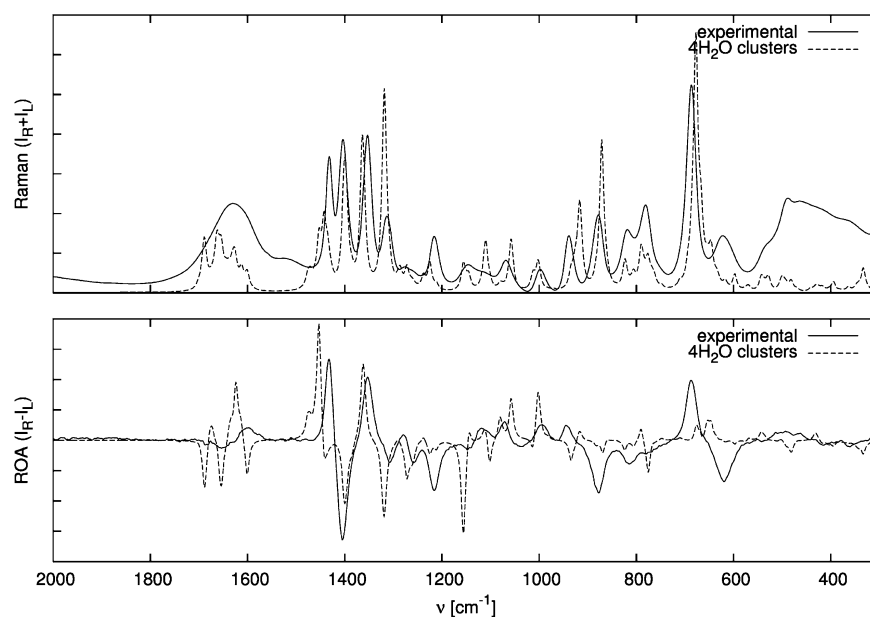


Figure 6. Comparison of the Raman (upper graph) and ROA (lower graph) obtained from optimized L-cysteine–water clusters with experiment.

experimental spectra, although the theoretical spectra are shifted in the direction of smaller wavenumber values for ca. 40 cm^{-1} . In the region from 900 to 1150 cm^{-1} , one can observe four peaks in the Raman spectrum, for which the assignment of corresponding theoretical peaks is not obvious, and corresponding four positive signals in the ROA spectrum from which only the last two (1070 , 1120 cm^{-1}) seem to be in agreement with the results of the calculation. Other bands that seem correctly calculated are found near 1210 and 1450 cm^{-1} . Two peaks at 1310 and 1350 cm^{-1} cannot be attributed to any of the theoretical ones with certainty, and in the region around 1600 cm^{-1} , this model seems to fail completely.

The calculated spectra exhibit some dependence on the IEF-PCM model employed. We have compared the performance of

the IEF-PCM model default in the 03 and 09 versions of the Gaussian program. As one can see in Figure S3 in the Supporting Information, there are shifts in vibrational frequencies as big as 20 cm^{-1} , and some of the Raman and ROA intensities are also affected (notably the region from 1300 to 1500 cm^{-1} : the ROA spectrum calculated with IEF-PCM as implemented in Gaussian 09 is even more discrepant with the experiment in this region than the results of Gaussian 03 calculations). Thus, the differences in implementations of the PCM in the two versions of the Gaussian package have a significant impact on the obtained vibrational spectra.

3. Explicit Solvation. *a. Microsolvation Model.* The Raman and ROA spectra obtained for cysteine–water clusters with optimized geometry are shown in Figure 6, which contains also the experimental spectrum.

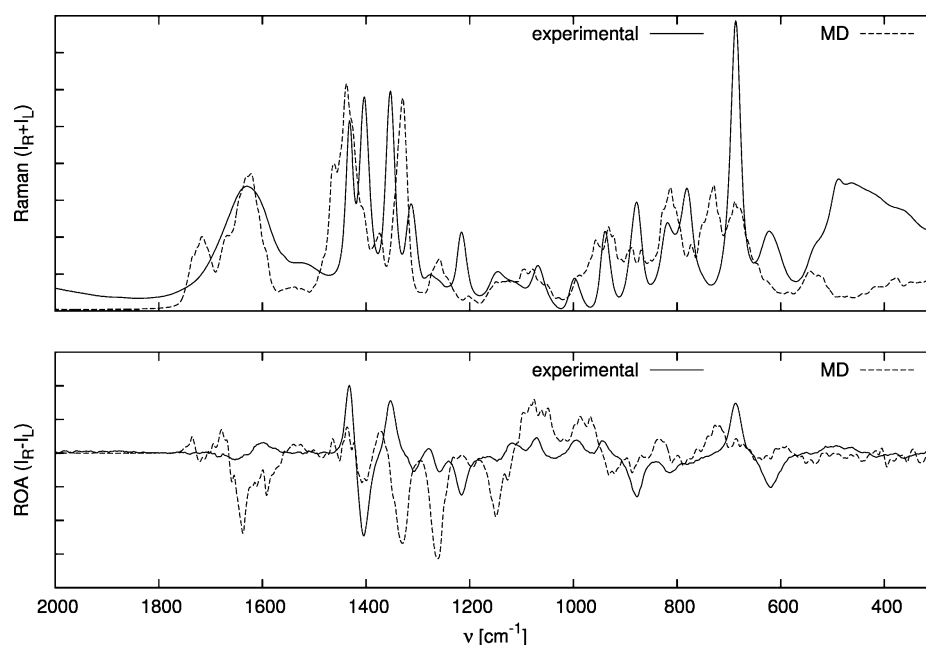


Figure 7. Comparison of the Raman (upper graph) and ROA (lower graph) spectra of L-cysteine obtained using the structures from the 5 ns MD simulation with experiment.

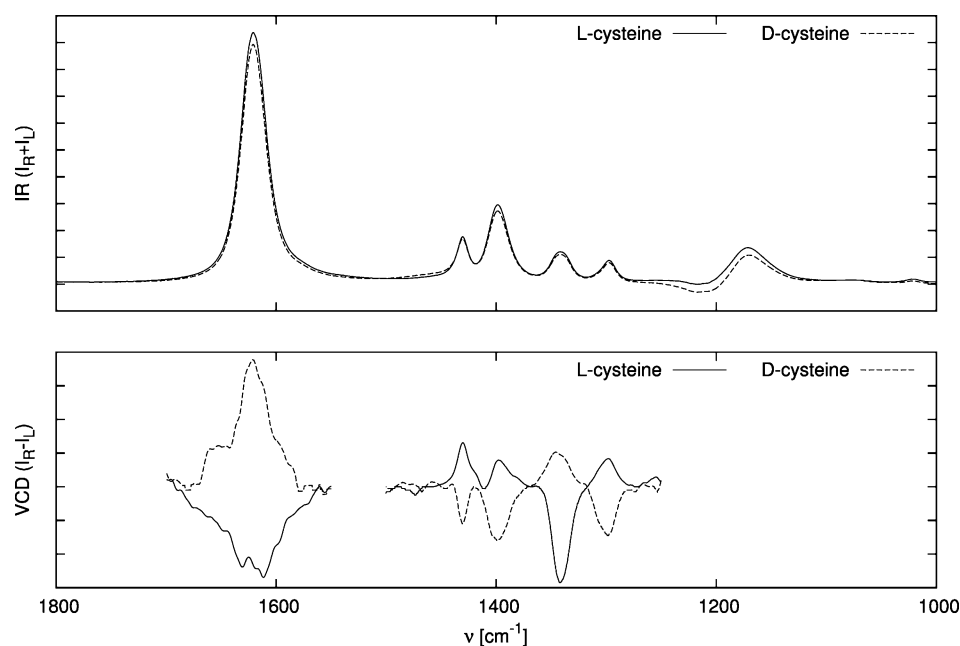


Figure 8. The IR (upper graph) and VCD (lower graph) spectra collected for heavy water solutions of L- and D-cysteine (1250–1500 cm^{-1} , saturated solution; 1550–1700 cm^{-1} , one-third of the concentration of saturated solution, spectral intensity multiplied by the factor of 3).

The ROA and especially the Raman spectrum obtained in this approach seem to be more in line with the experimental spectra than those from the implicit IEF-PCM approach. Almost every peak in the calculated Raman spectrum can be fairly easily assigned to a peak in the experimental spectrum, because the positions and intensities of the peaks match. The calculated ROA spectrum has a number of artifact signals, but up from 1000 cm^{-1} , it seems to follow the experimental spectrum. The exceptions are the strong peak at 1160 cm^{-1} , which is not present in the experimental spectrum and the peak at 1460 cm^{-1} , which seems to be shifted by ca. 25 cm^{-1} in the direction of higher wavenumbers. The broad band in the

experimental Raman spectrum between 1600 and 1700 cm^{-1} is now much more realistically reproduced by the calculations than when IEF-PCM is used, which is not surprising, as it comes mostly from water bending vibrations.

b. Molecular Dynamics Simulations. The alternative way to account for hydration by the explicit solvation model is to generate the clusters by molecular dynamics simulations and average them out. The results of such an approach for Raman and ROA spectra are compared with experimental spectra in Figure 7.

One can observe that in the case of both Raman and ROA spectrum the PCM-simulated spectrum is in much better

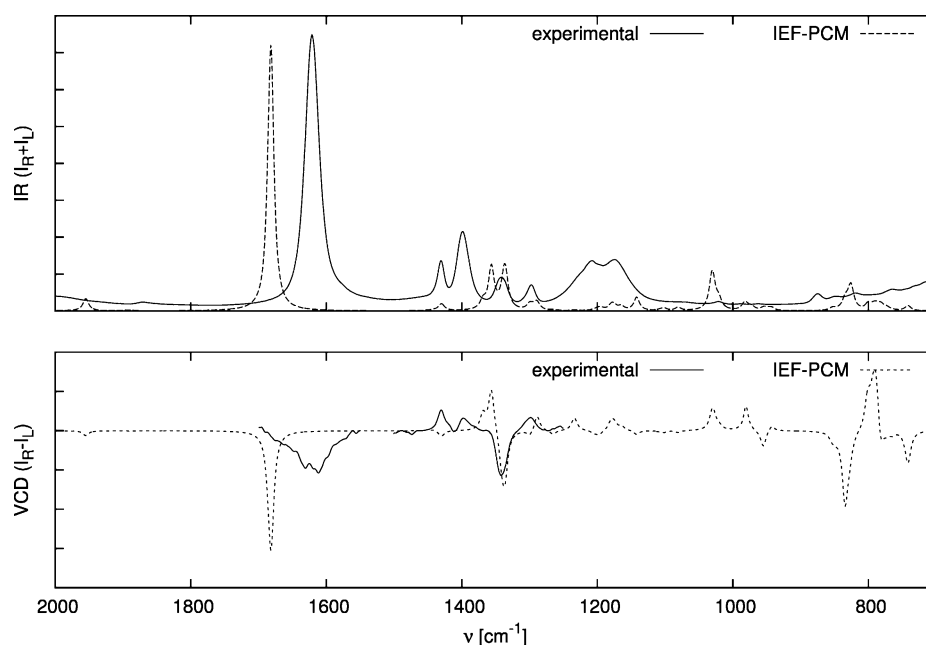


Figure 9. Comparison of the IR (upper graph) and VCD (lower graph) spectrum of L-cysteine obtained simulating aqueous environment by means of the IEF-PCM model (dashed line) with experiment (solid line).

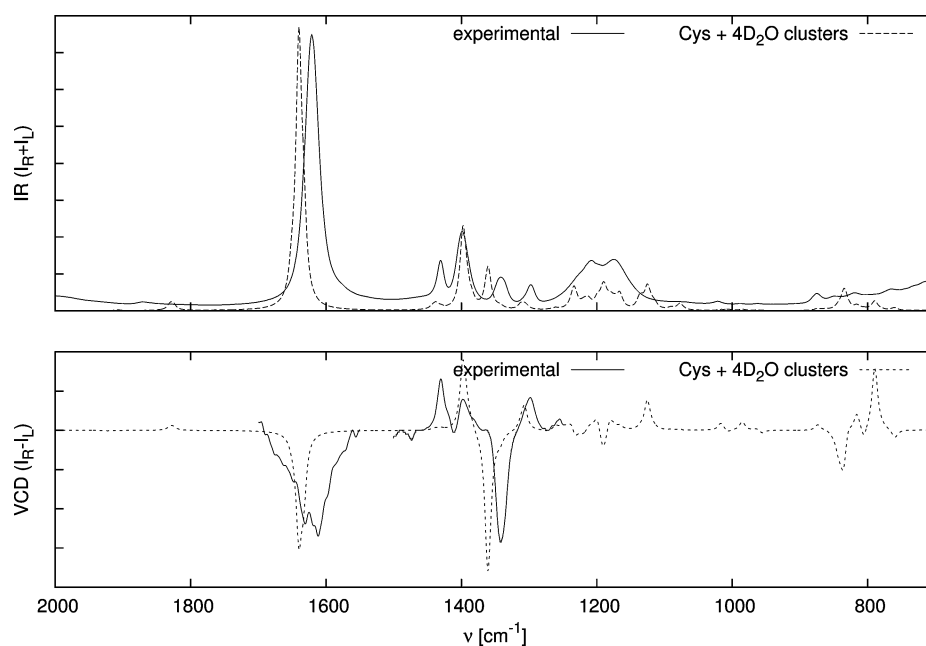


Figure 10. Comparison of the IR (upper graph) and VCD (lower graph) obtained from optimized L-cysteine–water clusters with experiment.

agreement with experiment than the MD one. (As discussed above, the agreement is better still for the microsolvation model.) The relative failure of our MD simulation to render the spectra of aqueous solution of cysteine is understandable, considering that the MD conformational distribution differs very much from the results of quantum chemical calculations. What is more, the spectra simulated from another set of MD snapshots, obtained from only 0.5 ns run and having more structures with $\beta \approx 300^\circ$ among them, are in much better agreement with experiment. This suggests that the AMBER02 force field used for the MD run is inappropriate for the purpose, which is not surprising, considering that it has been parametrized for the potential energy surface of an amino acid

moiety in a protein, rather than for a free molecule. On the other hand, as shown in ref 40, 100 MD snapshots are not sufficient for rendering of the ROA spectrum, but since it is the force field that is problematic, we decided not to pursue this way any further.

C. IR and VCD Spectra. 1. *Experimental Spectra.* The experimental IR and VCD spectra collected for heavy water solutions of L- and D-cysteine are shown in Figure 8. The VCD spectra of two enantiomers are close to being mirror images of each other, but due to the limited range of the VCD spectrometer, there are only four peaks clearly visible in the VCD spectra. The mirror symmetry is only approximate in the case of the 1621 cm^{-1} peak and it has been difficult to reproduce in

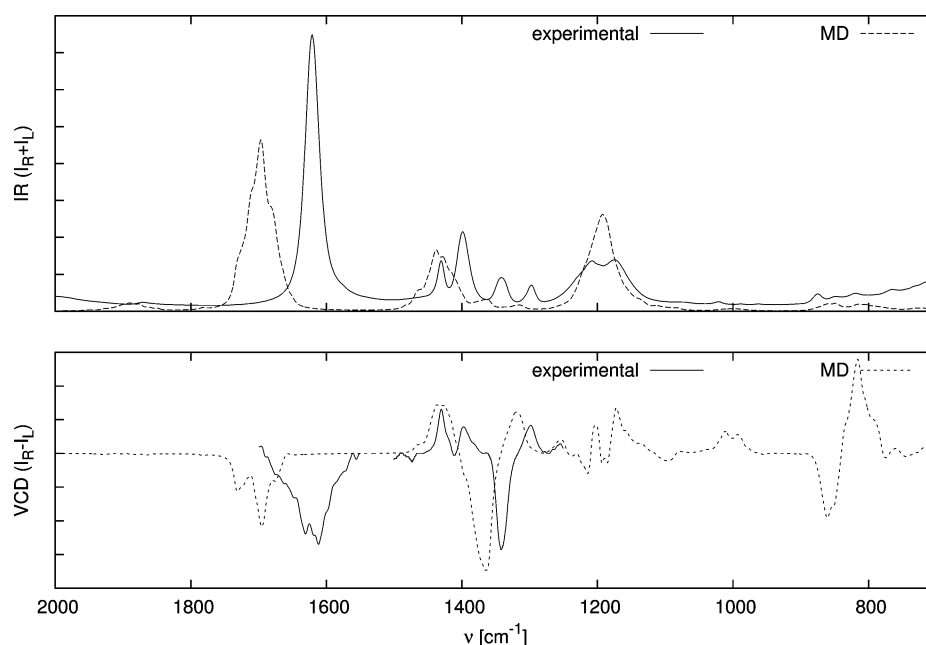


Figure 11. Comparison of the IR (upper graph) and VCD (lower graph) spectra obtained using the structures from the 5 ns MD simulations with experiment.

the VCD measurements. On the basis of the calculations for cysteine-heavy water clusters, the 1621 cm^{-1} peak in the IR spectrum can be ascribed mainly to the antisymmetric stretching vibration of the carboxyl group (see Table 2), the 1430 cm^{-1} peak to CH_2 scissoring vibrations, the 1399 and 1341 cm^{-1} peaks to symmetric stretching vibrations of the carboxyl group coupled in phase and in antiphase with the vibration changing the angle designated by H, C_α , and N atoms, and the 1298 cm^{-1} peak to the HC_α bending vibration in the plane that contains the $\text{C}_\alpha\text{C}_\text{O}$ bond coupled with wagging CH_2 vibrations. The calculation failed to reproduce the IR spectrum in the $1150\text{--}1250\text{ cm}^{-1}$ region, but the 1209 cm^{-1} peak matches the position of the heavy water IR absorption band, which suggests that the broad 1175 cm^{-1} peak may be attributed to ND_3 bending coupled with bending of D_2O molecules. The problem with reproducing the experimental spectrum in the region can also be attributed to the imperfect background subtraction.

2. Implicit Hydration Model. The experimental IR and VCD spectra and those calculated by means of the DFT/PCM model are shown in Figure 9 (upper and lower graph, respectively). As mentioned before, the range of wavenumbers in which the experimental VCD spectrum could be collected is more narrow than in the case of the other vibrational spectra, but we have shown it in the same range for easier comparison.

The agreement of the IR spectrum calculated using IEF-PCM with experiment is only approximate, mostly because the peaks are shifted in comparison with experiment. In the region around 1600 cm^{-1} in the calculated spectrum, there is one strong peak that can easily be assigned to the peak in the experimental spectrum, and in the region around 1400 cm^{-1} , in both experimental and theoretical spectra there are four peaks, but the intensities of the first two calculated peaks seem to be too low and the second one seems to be red-shifted by approximately 40 cm^{-1} .

The calculated VCD spectrum bears some resemblance to the experimental one, but a small number of peaks precludes more definite conclusions. The peak in the region around

Table 4. A Comparison of Molar Fractions of Cysteine Conformers Calculated with Boltzmann Distribution (Using ΔG) and Fitted^a

conformer	implicit hydration model		microsolvation model	
	$x_{\Delta G}$	x_{fit}	$x_{\Delta G}$	x_{fit}
a	0.502	0.57	0.225	0.34
b	0.228	0.00	0.134	0.00
c	0.135	0.43	0.070	0.36
d	0.061	0.00	0.504	0.06
e	0.075	0.00	0.066	0.24

^aIn the case of the microsolvation model, the molar fractions have been summed within each of the groups of structures derived from the same IEF-PCM conformer.

1600 cm^{-1} ($\nu_{\text{as}}(\text{COO}^-)$) seems to have its sign predicted correctly, and the same is true of the two peaks around 1300 and 1345 cm^{-1} , but this may be coincidental considering the ambiguity of peak assignment. Moreover, since the two peaks around 1360 and 1440 cm^{-1} in the calculated IR spectrum cannot be assigned unambiguously to the experimental ones, there is no way of telling whether the two other peaks in that region of the calculated VCD spectrum match the experiment or not.

To some extent, these problems are probably due to a particular range in which the experimental spectrum has been collected. For this region, in which there are large contributions from C–H bending vibrations, also the Raman and ROA bands are difficult to reproduce, as discussed in the subsection above and in ref 40. However, it is also possible that the VCD intensities are more affected than ROA by specific hydration effects. In order to examine the issue more closely, we have performed the calculations with an explicit presence of heavy water molecules, analogous to those performed for the ROA spectra with explicit H_2O .

3. Explicit Hydration Model. *a. Microsolvation Model.* The IR and VCD spectra calculated for the cysteine-heavy water cluster with optimized geometry are shown in Figure 10.

The spectra calculated in this approach seem more in agreement with experiment than for IEF-PCM-only calculations,

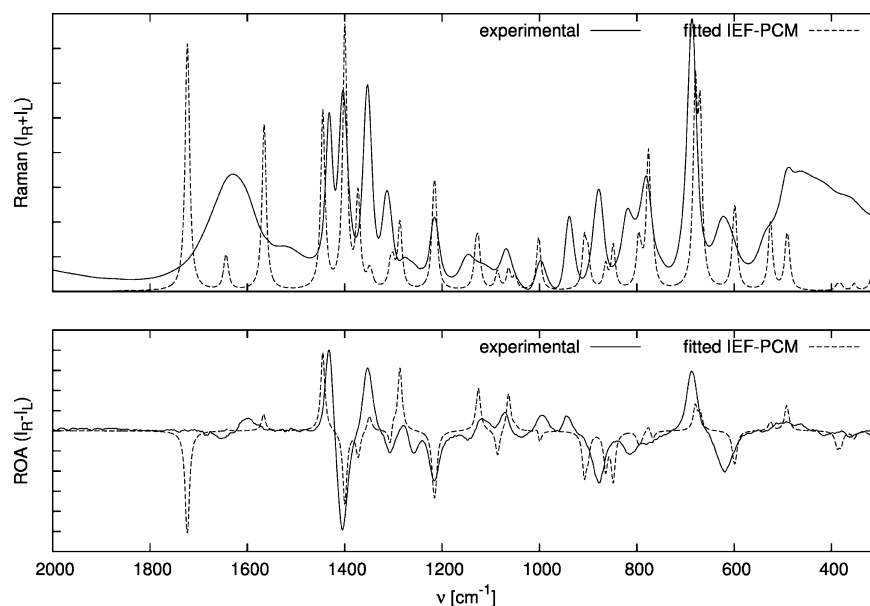


Figure 12. Comparison of the fitted ROA (lower graph) and Raman (upper graph) spectra of L-cysteine obtained using a linear combination of the theoretical spectra calculated with the IEF-PCM model with experiment.

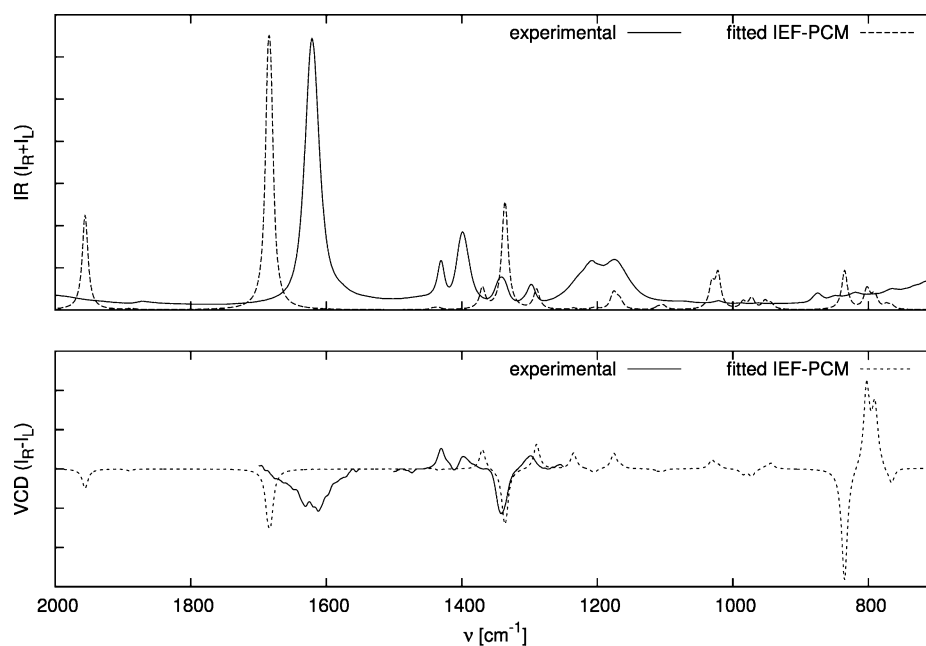


Figure 13. Comparison of the fitted IR (upper graph) and VCD (lower graph) spectra of L-cysteine obtained using a linear combination of the theoretical spectra calculated with the IEF-PCM model with experiment (fitting parameters from ROA).

mostly because the peak positions are now more or less correctly reproduced. The peak around 1600 cm^{-1} in the theoretic spectrum is a single peak and the structure, present in the experimental spectrum, is not visible. In the region around $1300\text{--}1400\text{ cm}^{-1}$, one can observe now four peaks, that could be assigned to the experiment as follows: the IR peak at ca. 1430 cm^{-1} in the calculated spectrum to the experimental signal at the same wave-number, the calculated peak at 1395 cm^{-1} to the experimental one at 1399 cm^{-1} , the peak calculated at 1355 cm^{-1} to the experimental one at 1342 cm^{-1} , and the peak calculated at 1303 cm^{-1} to the experimental one at 1298 cm^{-1} (compare also Table 2). The signs of these peaks in the VCD spectrum seem to be calculated properly, although their relative intensities are not.

b. Molecular Dynamics Simulations. The IR spectrum calculated for snapshots obtained in the course of MD simulation contains, as shown in Figure 11, a small number of broad bands. The band shapes seem somewhat better rendered than in the microsolvation model (for example, some structure of the broad band at 1600 cm^{-1} is visible), although their positions are not. The sign of the largest VCD band, corresponding to the COO^- stretching, is negative in experiment, and it seems to be correctly reproduced by means of all hydration models explored (IEF-PCM, microsolvation, and molecular dynamics), although the position of the band is shifted in the MD simulations in comparison with experiment. For the bands in the $1250\text{--}1550\text{ cm}^{-1}$ region, MD performs slightly better

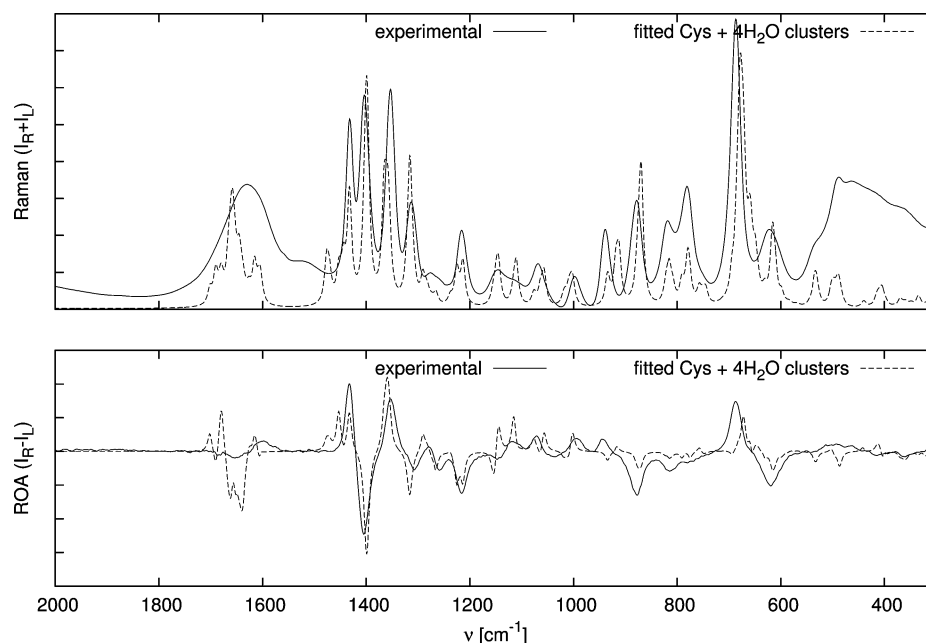


Figure 14. Comparison of the fitted ROA (lower graph) and Raman (upper graph) spectra of L-cysteine obtained using a linear combination of the theoretical spectra calculated with the microsolvation model with experiment.

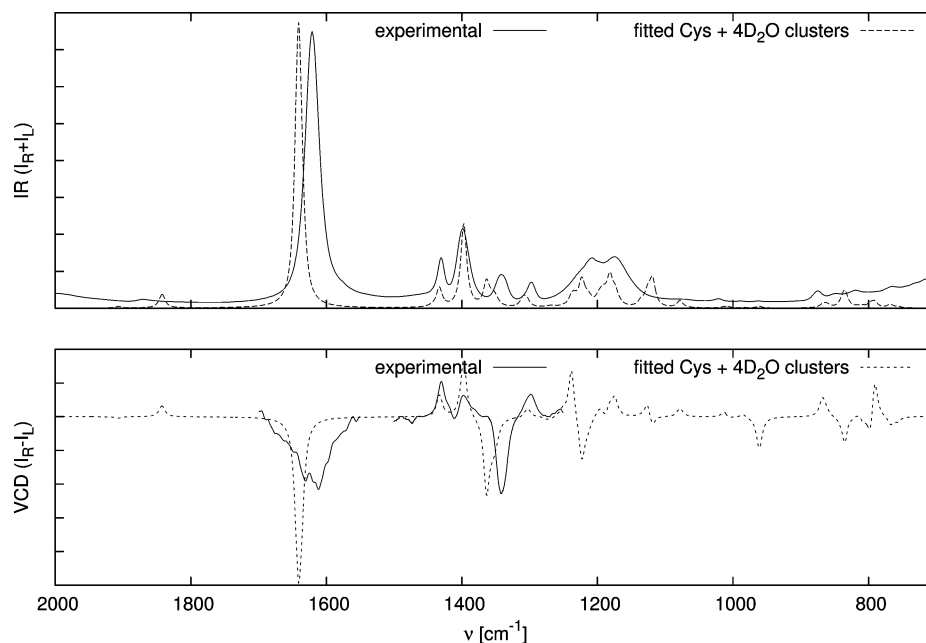


Figure 15. Comparison of the fitted IR (upper graph) and VCD (lower graph) spectra of L-cysteine obtained using a linear combination of the theoretical spectra calculated with the microsolvation model with experiment (fitting parameters from ROA).

than IEF-PCM but apparently worse than the microsolvation model. In the case of the next band, that at 1431 cm^{-1} (corresponding to 1430 cm^{-1} in the experimental spectrum), MD gives the correct positive sign, while IEF-PCM does not.

IV. FITTING OF THE SPECTRA

Now, we shall discuss how the chiroptical spectra calculated by means of quantum chemical methods can be used to obtain conformational ratios by comparison with experimental spectrum. For this purpose, linear combination of the calculated spectra has been used to fit the experimental spectra. The procedure has been applied for the ROA spectra, and the

resulting fitting parameters (which can be interpreted as conformational ratios) have been used to simulate Raman, IR, and VCD spectra as a quasi-independent verification of the obtained parameters.

A. Fitting Procedure. For each structure (or each group of structures with similar geometries in the case of the MD approach), the ROA spectra have been calculated (φ_n) and the Φ function has been minimized with respect to c_n fitting parameters, to fit to the experimental spectrum φ_{exp} .

$$\Phi = \int_{\nu_1}^{\nu_2} [\varphi_{\text{exp}} - \sum_n (c_n \cdot \varphi_n)]^2$$

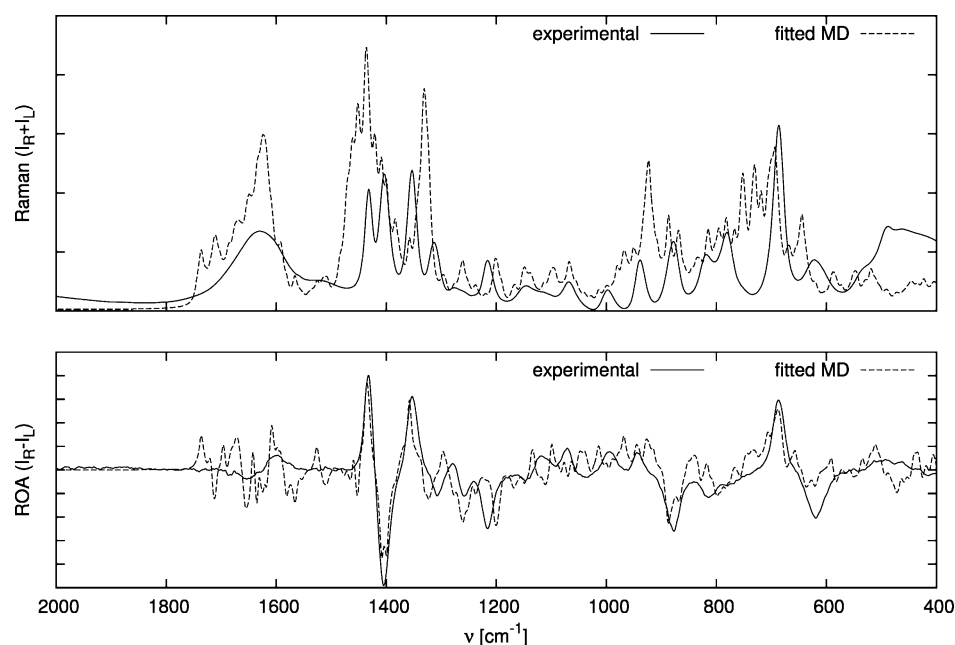


Figure 16. Comparison of the fitted ROA (lower graph) and Raman (upper graph) spectra of L-cysteine obtained using a linear combination of the theoretical spectra calculated from MD snapshots with experiment.

ν_1 and ν_2 in the above equation have been set to 600 and 1500 cm^{-1} , respectively. The exponent has been arbitrarily set to 4 to make sure that the Φ function is positive and that the contributions from weak peaks (which are more affected by numerical noise) are suppressed. The obtained c_n parameters correspond, after normalization to the sum of 1, to contributions of the ϕ_n spectra to the fitted spectrum and thus can be interpreted as the conformational ratios and, in the case of the implicit hydration model and the cysteine–water clusters approach, directly compared with the conformational ratios calculated from Boltzmann distribution factors.

B. Results of the Fitting Procedure. *1. Implicit Hydration Model.* Conformational ratios calculated during fitting of the ROA spectra of the five IEF-PCM conformers to the experimental spectrum have been presented in Table 4, and the fitted ROA and Raman spectra are shown in Figure 12. The fitted ROA spectrum is obviously close to the experimental one (since it has been used for the fitting procedure), but in the case of the Raman spectrum, there is little improvement over the spectrum calculated using theoretical Boltzmann distributions (compare Figures 12 and 5). This rather puts in doubt physical sense of this fitting. The molar fractions are 0.57 for the *a* conformer, 0.43 for the *c* conformer, and 0 for the rest of them (as shown in Table 4), so the *a* conformer is the most abundant one, similarly as in theoretical calculations. However, the *c* conformer, predicted as the second conformer dominating the spectrum, has the Boltzmann distribution of only 0.13. What is worth pointing out, both conformers with nonzero fitted contributions have the β angle around 300° , and the conformer *b* with β angle of 188° , which, according to the theoretical predictions is the second in energy, is not populated at all.

The ROA fitted molar fractions have also been used to calculate the IR and VCD spectra of deuterated conformers, assuming that the conformational ratios are identical as for nondeuterated cysteine (which is obviously an approximation but, judging from the data in Table 1, a justified one). The resulting spectra are shown in Figure 13. Like for the Raman

spectrum, the improvement over the spectra calculated using theoretical Boltzmann distributions is disputable. Thus, we conclude that the molar fractions obtained by fitting theoretical ROA spectra obtained with the IEF-PCM model to the experimental spectrum are not physical.

2. Microsolvation Model. Molar fractions calculated during fitting of the ROA spectrum of the cysteine–water clusters have been presented in Table 4 and the fitted ROA and Raman spectra in Figure 14. The fitted ROA spectrum is closer to the experimental data than in the previous case, and, what is particularly gratifying, the same is true for the Raman spectrum. After adding the resulting molar fractions of the clusters constructed from each of the IEF-PCM conformers, the summary molar fractions are somewhat similar to those obtained previously: 0.34 for *a*-, 0 for *b*-, 0.36 for *c*-, 0.06 for *d*-, and 0.24 for *e*-derived structures. According to the fitting procedure, the conformers *c* and *a* are the most abundant ones, in agreement with the results from fitting of IEF-PCM spectra (see above), but in variance with theoretical predictions for cysteine–water cluster. As the geometries of the cysteine molecules in the clusters have not practically changed after addition of the water molecules and the geometry optimization, again, most of the conformers with nonzero fitted contributions have the β angle around 300° . The exception here is the *e*-5 structure, which has $\alpha = 0.24$ and $\beta = 184^\circ$.

The ROA fitted molar fractions have been used to calculate the IR and VCD spectra of Cys-4D₂O clusters (Figure 15), assuming again that deuteration does not change the conformational ratios. This resulted in very good correlation between the fitted and experimental VCD and IR spectra, which suggests that the predictions of conformational ratios from “microsolvation spectra” are more reliable than from IEF-PCM. This also constitutes a further confirmation that the microsolvation model is superior over IEF-PCM (and, as it will be discussed below, to MD with the AMBER02 force field.)

3. Molecular Dynamics Simulations. Each conformer obtained from the 5 ns MD simulation and normal mode optimization has been classified into one of the groups obtained by

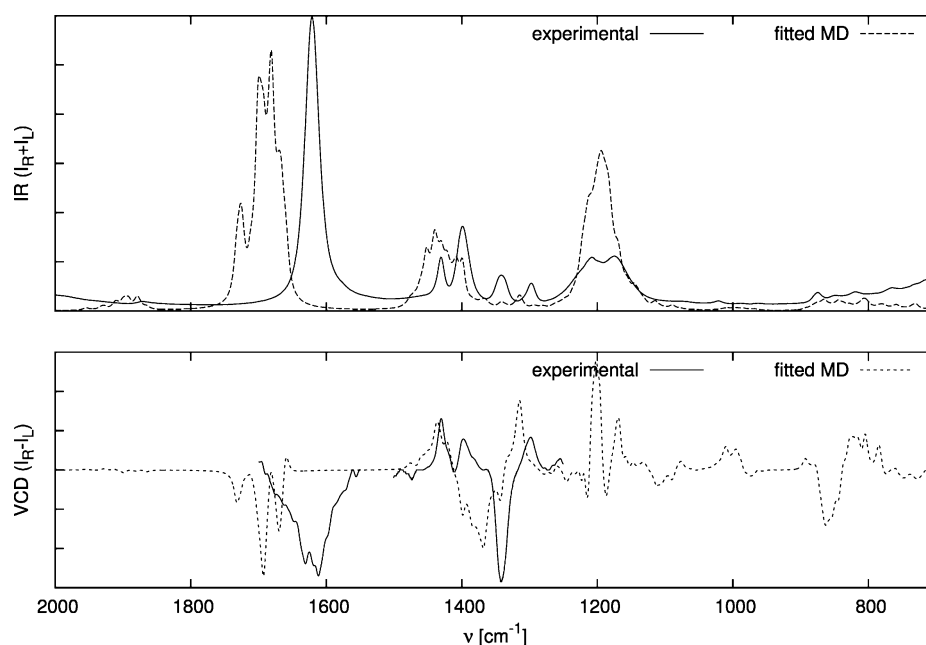


Figure 17. Comparison of the fitted IR (upper graph) and VCD (lower graph) spectra of L-cysteine obtained using a linear combination of the theoretical spectra calculated from MD snapshots with experiment (fitting parameters from ROA).

dividing the α , β , γ , and δ dihedral angles into 30° increments. This procedure resulted in 71 populated groups. Comparison of the experimental ROA spectrum with the ROA spectrum that has been fitted to the experimental one by varying the contributions of the groups of MD snapshots with similar geometry to the final ROA spectrum is shown in Figure 16. Since it has been fitted to the experimental one, the ROA spectrum matches it fairly well. Unfortunately, that is not the case with the Raman spectra and both calculated ROA and Raman spectra are quite noisy, which can partly be attributed to the lack of flexibility of the fitting procedure to fit slightly shifted peaks. Nonzero contributions of groups of the MD structures have been listed in Table S3 in the Supporting Information. Again, the structures with the highest contribution to the fitted ROA spectrum are those in which the β torsion angle is equal approximately to 300° . Thus, it is not surprising that the MD simulation rendered such poor results: the conformers with β around 300° are significantly underrepresented there in comparison with IEF-PCM simulation (compare Table 1 for IEF-PCM) or the microsolvation model (compare Table S2 in the Supporting Information).

The ROA fitted molar fractions have again been used to calculate the IR and VCD spectra for those obtained from the MD structures (Figure 17). This results in the spectra which are rather noisy and do not seem to correlate well with the experimental ones. Thus, the conformer ratios extracted by fitting the MD spectra to the experimental one have little physical meaning.

V. SUMMARY AND CONCLUSIONS

The Raman, Raman optical activity, infrared, and vibrational circular dichroism spectra of cysteine in aqueous solution (D_2O in the case of IR and VCD spectra) have been measured and calculated by means of density functional theory. The influence of aqueous environment on the spectra has been simulated by means of the polarizable continuum model

in IEF-PCM implementation, the microsolvation model employing $Cys \cdot 4D_2O$ clusters, and classical molecular dynamics with the AMBER02 force field. The linear combination of the calculated spectra has been used to fit the experimental spectra, and the fitting parameters can be interpreted as conformational ratios.

The results indicate that, while PCM reproduces some of the features of the spectra, the best description is consistently rendered by the microsolvation model combined with PCM. The shape of the bands is in some cases more correctly reproduced by MD, but their intensities and positions are not, since these simulations are hampered by the standard force field being parametrized for conformations of peptides rather than isolated amino acids. The VCD spectrum has been found to be rather more difficult to reproduce by theoretical calculations than the ROA one, but this may be due to a particular range in which the experimental VCD spectrum has been collected, in which also the other vibrational spectra under study are discrepant with experiment. This region, dominated by the C–H bending modes, has been found to be difficult to simulate also in the previous work.⁴⁰

The calculated ROA spectra have been used to extract conformational ratios from the experimental spectra, and the best results (as verified by simulations of other spectra) have been obtained when using the microsolvation model. According to this procedure, there are three zwitterion conformers dominating the spectra of hydrated cysteine, of conformational ratios of 35% (*c*), 33% (*a*), and 24% (*e*), respectively. The conformer *a* has been found to have the lowest energy in the theoretical IEF-PCM calculations, while the *c* and *e* conformers are third and fifth in the energy scale, respectively. The *a* and *c* conformers have the $SC_\beta C_\alpha N$ dihedral angle of about 300° , and underrepresentation of these conformers in the course of MD simulation is the cause of relative failure of MD to reproduce the experimental spectra.

■ ASSOCIATED CONTENT

■ Supporting Information

The energy, free enthalpy, and mole fractions of the cysteine conformers as calculated using the PCM version available in Gaussian 09 (Table S1), the energy, free enthalpy, and mole fractions of the explicitly hydrated cysteine conformers (Table S2), the fitted contributions of groups of the MD structures (Table S3), the structures of the explicitly hydrated cysteine conformers (Figure S1), the comparison of Raman and ROA spectra for 1 and 0.25 M cysteine solutions (Figure S2), and the comparison of Raman and ROA spectra as calculated using the PCM versions available in Gaussian 03 and 09 (Figure S3). This material is available free of charge via the Internet at <http://pubs.acs.org>.

■ AUTHOR INFORMATION

Corresponding Author

*E-mail: mpecul@chem.uw.edu.pl.

Notes

The authors declare no competing financial interest.

■ ACKNOWLEDGMENTS

The work has been financed by the Ministry of Science and Higher Education (Poland) from funds for scientific research in years 2009–2011 as project No. N N204 138637 and has received support from the Wrocław Centre for Networking and Supercomputing through a grant of computer time. The study has been carried out using the research equipment purchased under CePT project cofinanced by European Union from the European Regional Development Fund under the Operational Programme Innovative Economy 2007–2013.

■ REFERENCES

- (1) McCann, D. M.; Stephens, P. J.; Cheeseman, J. R. *J. Org. Chem.* **2004**, *69*, 8709–8717.
- (2) Stephens, P. J.; McCann, D. M.; Butkus, E.; Stončius, S.; Cheeseman, J. R.; Frisch, M. J. *J. Org. Chem.* **2004**, *69*, 1948–1958.
- (3) Polavarapu, P. L. *Angew. Chem., Int. Ed.* **2002**, *41*, 4544–4546.
- (4) Costante, J.; Hecht, L.; Polavarapu, P. L.; Collet, A.; Barron, L. D. *Angew. Chem., Int. Ed. Engl.* **1997**, *36*, 885–887.
- (5) He, J. T.; Petrovich, A.; Polavarapu, P. L. *J. Phys. Chem. A* **2004**, *108*, 1671–1680.
- (6) Stephens, P. J.; Devlin, F. J.; Cheeseman, J. R.; Frisch, M. J.; Bortolini, O.; Besse, P. *Chirality* **2003**, *15*, S57–S64.
- (7) Zuber, G.; Hug, W. *Helv. Chim. Acta* **2004**, *87*, 2208–2234.
- (8) Haesler, J.; Schindelholtz, L.; Riguet, E.; Bochet, C.; Hug, W. *Nature* **2007**, *446*, 526–529.
- (9) Lovchik, M. A.; Frater, G.; Goeke, A.; Hug, W. *Chem. Biodiversity* **2008**, *5*, 126–139.
- (10) Gheorghe, R.; Chamoreau, L. M.; Kapitan, J.; Ovanesyan, N. S.; Aldoshin, S. M.; Hecht, L.; Barron, L. D.; Train, C.; Gruselle, M. *Chirality* **2007**, *20*, 1085–1091.
- (11) Polavarapu, P. L. *Chirality* **2008**, *20*, 664–672.
- (12) Polavarapu, P. L. *Chem. Rec.* **2007**, *7*, 125–136.
- (13) Freedman, T. B.; Cao, X.; Oliveira, R. V.; Cass, Q. B.; Nafie, L. A. *Chirality* **2003**, *15*, 196–200.
- (14) Freedman, T. B.; Cao, X.; Dukor, R. K.; Nafie, L. A. *Chirality* **2003**, *15*, 743–758.
- (15) Buděšínský, M.; Daněček, P.; Bednářová, L.; Kapitán, J.; Baumruk, V.; Bouř, P. *J. Phys. Chem. A* **2008**, *112*, 8633–8640.
- (16) Buděšínský, M.; Sebestník, J.; Bednářová, L.; Baumruk, V.; Safarik, M.; Bouř, P. *J. Org. Chem.* **2008**, *73*, 1481–1489.
- (17) Pecul, M. *Chirality* **2009**, *21*, E98–E104.
- (18) Devlin, F. J.; Stephens, P. J.; Österle, C.; Wiberg, K. B.; Cheeseman, J. R.; Frisch, M. J. *J. Org. Chem.* **2002**, *67*, 8090–8096.
- (19) Keiderling, T. A. *Curr. Opin. Chem. Biol.* **2002**, *6*, 682–688.
- (20) Cappelli, C.; Monti, S.; Rizzo, A. *Int. J. Quantum Chem.* **2005**, *104*, 744–757.
- (21) Zhu, F.; Isaacs, N. W.; Hecht, L.; Barron, L. D. *Structure* **2005**, *13*, 1409–1419.
- (22) Blanch, E. W.; Hecht, L.; Barron, L. D. *Methods* **2003**, *29*, 196.
- (23) Zhu, F.; Tranter, G. E.; Isaacs, N. W.; Hecht, L.; Barron, L. D. *J. Mol. Biol.* **2006**, *363*, 19–26.
- (24) Barron, L. D.; Hecht, L.; Blanch, E. W.; Bell, A. F. *Prog. Biophys. Mol. Biol.* **2000**, *73*, 1–49.
- (25) Wang, L.; Pancoska, P.; Keiderling, T. A. *Biochemistry* **1994**, *33*, 8428–8435.
- (26) Polyanichko, A.; Wieser, H. *Spectroscopy* **2010**, *24*, 239–244.
- (27) Yamamoto, S.; Straka, M.; Watarai, H.; Bour, P. *Phys. Chem. Chem. Phys.* **2010**, *12*, 11021–11032.
- (28) Cappelli, C.; Corni, S.; Mennucci, B.; Cammi, R.; Tomasi, J. *J. Phys. Chem. A* **2002**, *106*, 12331–12339.
- (29) Wang, F.; Zhao, C.; Polavarapu, P. L. *Biopolymers* **2004**, *75*, 85–93.
- (30) Pecul, M.; Lamparska, E.; Cappelli, C.; Frediani, L.; Ruud, K. *J. Phys. Chem. A* **2006**, *110*, 2807–2815.
- (31) Debie, E.; Bultinck, P.; Herrebout, W.; van der Veken, B. *Phys. Chem. Chem. Phys.* **2008**, *10*, 3498–3508.
- (32) Tomasi, J.; Persico, M. *Chem. Rev.* **1994**, *94*, 2027–2094.
- (33) Tomasi, J.; Mennucci, B.; Cammi, R. *Chem. Rev.* **2005**, *105*, 2999–3094.
- (34) Cammi, R.; Mennucci, B.; Tomasi, J. In *Computational Chemistry, Review of Current Trends*; Leszczynski, J., Ed.; World Scientific: Singapore, 2003; Vol. 8.
- (35) Klamt, A.; Schüürmann, G. *J. Chem. Soc., Perkin Trans. 2* **1993**, 799–805.
- (36) Klamt, A. *J. Phys. Chem.* **1995**, *99*, 2224–2235.
- (37) Klamt, A.; Jonas, V. *J. Chem. Phys.* **1996**, *105*, 9972–9980.
- (38) Wesolowski, T. A. *Int. J. Mod. Phys. C* **1991**, *2*, 531–535.
- (39) Jensen, L.; van Duijnen, P. T.; Snijders, J. G. *J. Chem. Phys.* **2003**, *118*, 514–521.
- (40) Hopmann, K. H.; Ruud, K.; Pecul, M.; Kudelski, A.; Dračinský, M.; Bouř, P. *J. Phys. Chem. B* **2011**, *115*, 4128–4137.
- (41) Kubelka, J.; Huang, R.; Keiderling, T. A. *J. Phys. Chem. B* **2005**, *109*, 8231–8243.
- (42) Šebek, J.; Kapitaán, J.; Šebestík, J.; Baumruk, V.; Bouř, P. *J. Phys. Chem. A* **2009**, *113*, 7760–7768.
- (43) Cheeseman, J. R.; Majeed, S. S.; Popelier, P. L. A.; Blanch, E. W. *J. Am. Chem. Soc.* **2011**, *133*, 4991–4997.
- (44) Pecul, M. *Chem. Phys. Lett.* **2006**, *427*, 166–176.
- (45) Osinska, K.; Pecul, M.; Kudelski, A. *Chem. Phys. Lett.* **2010**, *496*, 86–90.
- (46) Gargaro, A. R.; Barron, L. D.; Hecht, L. *J. Raman Spectrosc.* **1993**, *24*, 91–96.
- (47) Sadlej, J.; Dobrowolski, J. C.; Rode, J. E.; Jamróz, M. H. *J. Phys. Chem. A* **2007**, *111*, 10703–10711.
- (48) Graff, M.; Bukowska, J. *J. Phys. Chem. B* **2005**, *109*, 9567–9574.
- (49) Hug, W.; Hangartner, G. A. *J. Raman Spectrosc.* **1999**, *30*, 841–852.
- (50) Hug, W. *Appl. Spectrosc.* **2003**, *57*, 1.
- (51) Abdali, S. *J. Raman Spectrosc.* **2006**, *37*, 1341–1345.
- (52) Shaw, R. A.; Wieser, H.; Dutler, R.; Rauk, A. *J. Am. Chem. Soc.* **1990**, *112*, 5401–5410.
- (53) Berthier, D.; Buffeteau, T.; Léger, J.; Oda, R.; Huc, I. *J. Am. Chem. Soc.* **2002**, *124*, 13486–13494.
- (54) Cannan, R. K.; Knight, B. C. *J. G. Biochem. J.* **1927**, *21*, 1384–1390.
- (55) Gronert, S.; O'Hair, R. A. *J. Am. Chem. Soc.* **1995**, *117*, 2071–2081.
- (56) Dobrowolski, J. C.; Rode, J. E.; Sadlej, J. *J. Mol. Struct.* **2007**, *810*, 129–134.
- (57) Frisch, M. J.; Trucks, G. W.; Schlegel, H. B.; Scuseria, G. E.; Robb, M. A.; Cheeseman, J. R.; Montgomery, J. A., Jr.; Vreven, T.; Kudin, K. N.; Burant, J. C.; et al. *Gaussian 03*, revision a.1; Gaussian, Inc.: Wallingford, CT, 2003.

(58) Frisch, M. J.; Trucks, G. W.; Schlegel, H. B.; Scuseria, G. E.; Robb, M. A.; Cheeseman, J. R.; Scalmani, G.; Barone, V.; Mennucci, B.; Petersson, G. A.; et al. *Gaussian 09*, revision A.1; Gaussian, Inc.: Wallingford, CT, 2009.

(59) Ponder, J. W. *Tinker - software tools for molecular design*, version 5.1; 2010.

(60) Bouř, P.; Keiderling, T. A. *J. Chem. Phys.* **2002**, *117*, 4126–4132.

(61) Susi, H.; Byler, D. M.; Gerasimowicz, W. V. *J. Mol. Struct.* **1983**, *102*, 63–79.